Reactions of Trimethylindium on TiO_2 Nanoparticles: Experimental and Computational Study

Jeng-Han Wang and M. C. Lin*

Department of Chemistry, Emory University, Atlanta, Georgia 30322

Received: February 21, 2005; In Final Form: May 23, 2005

This article reports the results of an experimental and computational study on the reaction of trimethylindium, $In(CH_3)_3$, adsorbed on TiO_2 nanoparticle films. Experimentally, Fourier transform infrared (FTIR) spectra have been measured by varying $In(CH_3)_3$ dosing pressure, UV irradiation time in the absence and presence of oxygen, and surface annealing temperature on both "clean" and HO-covered TiO_2 nanoparticle films. Computationally, adsorption energies, molecular structures, and vibrational frequencies of possible adsorbates have been predicted by first-principles calculations based on the density functional theory (DFT) and the pseudopotential method. Three important reactions involving CH_3 elimination, CH_4 elimination, and CH_3 migration from the adsorbed trimethylindium have been elucidated in detail. CH_3 migration is the only exothermic process with the lowest reaction barrier. On the basis of experimental and computational results, the two sharpest peaks at 2979 and 2925 cm^{-1}, detected in the dosage and UV irradiation experiments in the absence of oxygen, are attributable to the asymmetric and symmetric C−H vibrations of methyl groups in $In(CH_3)_3$(a) and its derivatives, $(H_3C)_2In$(a), H_3CIn(a), and H_3CO(a). In the UV irradiation experiment in the presence of oxygen, the methyl groups attached to the In atom were quickly oxidized to the methoxy with the C−H vibrations at 2925 and 2822 cm^{-1} and to the carboxyl group with vibrations at 2888 cm^{-1} (υ_s(CH)), 1577 cm^{-1} (υ_a(OCO)), 1380 cm^{-1} (δ(CH)), and 1355 cm^{-1} (υ_s(OCO)). Finally, from the computed energies with vibrational analysis, the adsorbed structure of the carboxyl group was confirmed to involve two oxygen atoms doubly adsorbed on two surface Ti atoms.

1. Introduction

TiO_2 has been widely studied because of its unique photochemical characteristics for potential applications spanning from photocatalysis to wet solar cells and photoelectrochemical water splitting.[1−5] Recently, we have shown that indium nitride, InN, deposited on 20 nm TiO_2 nanoparticle films by low-pressure organometallic chemical vapor deposition (OMCVD) process[6] exhibits a broad UV/visible absorption between 390 and 800 nm quite similar to Graetzel's "black" dye,[7] indicating a promising possibility for photovoltaic applications. Understanding the surface reactions between the precursors, hydrazoic acid (HN_3) and trimethylindium (TMIn), and the TiO_2 substrate can help us elucidate the chemistry involved in the InN film deposition by OMCVD. The reaction of hydrazoic acid with TiO_2 nanoparticle films has been studied in our recent work,[8] and that of TMIn with TiO_2 is presented in this paper.

TMIn is considered to be one of the most efficient indium precursors in manufacturing of indium-containing semiconductors by OMCVD and molecular beam epitaxial (MBE) processes.[9−12] These products are widely used for photovoltaic and optoelectronic applications, such as InN for solar cell and electronic sensors,[13−15] InGaN for laser diode and light emitter products,[16−18] InAsN for optical fibers,[19] and InP for photodiodes and photovoltaic devices.[5,20]

Various reactions of TMIn on semiconductor surfaces have been widely studied. On the quartz surface, photodissociation of the adsorbed TMIn at 222 nm had been investigated at 150 K and its photofragments, $In(CH_3)_2$, $InCH_3$, In, and CH_3, were detected by time-of-flight mass spectroscopy (TOF/MS).[21,22] On the GaAs(100) surface, the thermal decomposition of TMIn was studied by high-resolution energy loss spectroscopy (HREELS)[23,24] and X-ray photoelectron spectroscopy (XPS),[25] and the photodissociation reaction at 193 nm was studied by angle-resolved XPS.[26] The results showed that the weaker In−C bond cleavage of the adsorbed TMIn was observed at 300 K or dissociated by 193 nm laser irradiation at 150 K. This decomposition process took place via an exchange reaction in which the methyl groups switch from In to Ga due to the stronger Ga−C bond. On the Si(111) surface, the photodissociation at 193 nm[27] and thermal decomposition studies[28] showed that the adsorbed species include indium metal and CH_x species on the surface resulting from the In−C bond cleavage. At temperatures above 950 K, SiC was the only adsorbate left on the surface. Generally speaking, TMIn chemically adsorbs on the surfaces at low temperature, ∼150 K. The weaker In−C bond of the adsorbed TMIn may be broken at higher surface temperature, ∼300 K, or by UV irradiation. The adsorbed TMIn fragments further decompose to CH_x(a), C(a), H(a), and In(a) species at higher surface temperatures.

In this paper, the adsorption and reactions of TMIn on 15−20 nm TiO_2 nanoparticle films have been investigated by Fourier transform infrared (FTIR) experiments aided by first-principle calculations. The experimental setup with FTIR spectroscopy is presented in section 2. The results of these FTIR experiments, which were carried out by systematically examining the effects of TMIn dosage, UV irradiation in the absence of oxygen, UV irradiation in the presence of oxygen, and surface temperature,

* To whom correspondence should be addressed. E-mail: chemmcl@emory.edu.

10.1021/jp050892v CCC: $30.25
Published on Web 10/15/2005

are presented in section 3. The computational method used for the slab surface model is presented in section 4. These calculated results, including the optimized structures, adsorption energies, potential energy surfaces, and vibrational frequencies, are rationalized with the experimental observations and discussed in section 5. This paper is concluded in section 6 with a brief summary.

2. Experimental Setup

The preparation of TiO_2 nanoparticles by the sol−gel method, similar to that reported by Zaban and co-workers,[29] was carried out by the controlled hydrolysis of titanium(IV) isopropoxide, $Ti(i\text{-}OC_3H_7)_4$ (Aldrich 97%), in a mixture of glacial acetic acid and water at 273 K. The resulting solution was heated to 353 K for 8 h and then autoclaved at 503 K for 12 h. Then the transformed TiO_2 sol−gel solution was spread onto a tungsten grid (Alfa Aesar) and baked in an oven at 723 K to form TiO_2 nanoparticle films with sizes in the range of 15−20 nm as measured by scanning electron microscopic and atomic force microscopic images.[6] To increase the adhesion between TiO_2 nanoparticles and tungsten grids, the film in the IR cell was then heated to 900 K under vacuum for 24 h. To remove the small amount of organic contaminants and to fill oxygen vacancies in TiO_2, the film (denoted as "clean" film hereafter) was annealed at 673 K in a vacuum with 2 Torr of oxygen for 2 h prior to every experiment. It should be noted that our InN films were also deposited previously on TiO_2 nanoparticles of the same 15−20 nm size.

TMIn purchased from Strem with 98+% purity was stored in a Pyrex tube after vacuum distillation. The effusive beam source, from the vapor over the crystalline TMIn at room temperature, was introduced into the system through a 1/8-in. stainless steel tube above the substrates. The gas flow rate monitored by a low-pressure transducer (MSK Baratron) was controlled by combined needle and shutoff valves.

The vacuum system setup, similar to the one employed by Basu et al.,[30] was described in detail previously.[8] Briefly, a stainless steel IR cell with two CaF_2 windows sealed by Viton O-rings and one UV-grade sapphire window was connected to a high-vacuum chamber with a base pressure of 1×10^{-7} Torr. TiO_2 nanoparticle film supported on a tungsten grid was held rigidly by a power/thermocouple feedthrough and could be resistively heated to 900 K. The spectra presented in this paper were measured by a Bruker IFS66 FTIR spectrometer equipped with an MCT detector and had been subtracted by the background spectrum of a "clean" TiO_2 nanoparticle film. The entire optical path was purged with dry air passing through H_2O- and CO_2-free filters (Ballston). A 1000 W high-pressure Hg-(Xe) arc lamp (Oriel) was used as the UV light source ($\lambda \geq$ 200 nm). The intensity of the UV light beam used for current photochemical experiments could be varied up to 2.0 W/cm^2 as measured in air inside the IR cell with a power meter.

3. Experimental Results and Discussion

The following four subsections discuss the $In(CH_3)_3$ dosage, UV irradiation in the absence of oxygen, UV irradiation in the presence of oxygen, and surface annealing experiments, respectively. Each series of experiments was carried out on the "clean" and the HO-covered surfaces. The "clean" surface prepared as described in the Experimental Section was applied as the background scan in the FTIR experiments. The HO-covered surface was prepared by exposing 2 Torr of water vapor on the "clean" surface for 10 min, evacuating for 30 min, and then heating the surface to 373 K for 5 min. After the heating process,

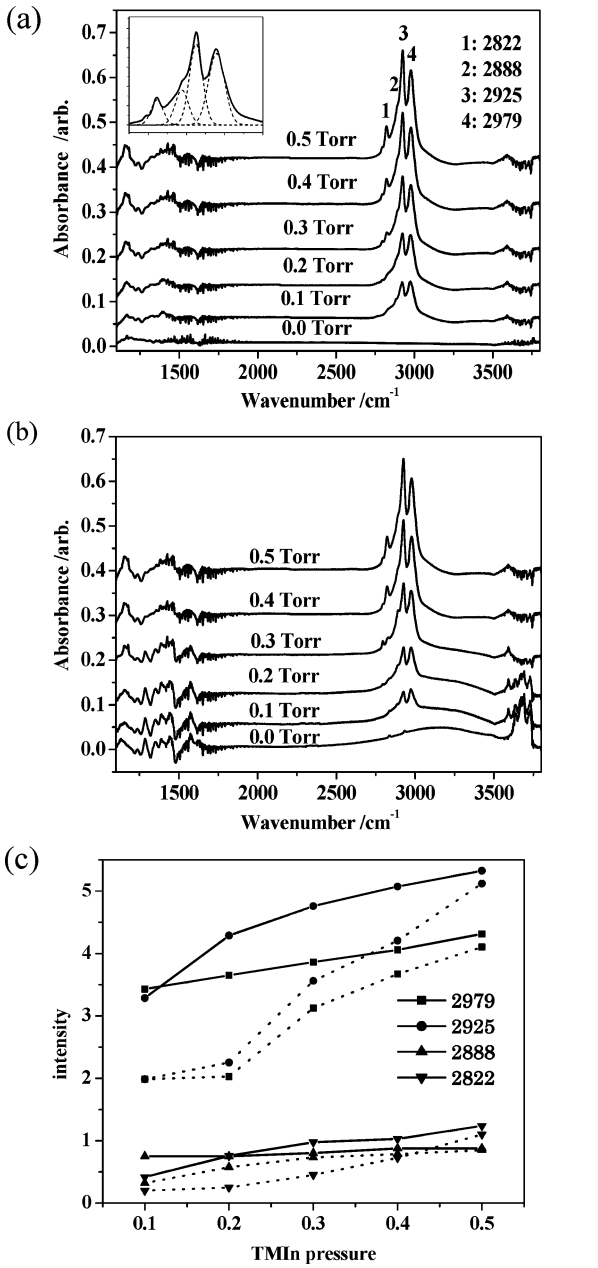

Figure 1. FTIR spectra of the dosing experiment on (a) "clean" and (b) HO-covered TiO_2 nanoparticle films. (c) Plots of peak areas as a function of dosing pressure. Solid and dotted lines represent the changes of the "clean" and HO-covered surfaces, respectively.

the molecularly adsorbed water was removed and pure HO-covered surface was formed. This HO-covered surface was confirmed by the disappearance of the water bending mode at ca. 1620 cm^{-1} and the remaining associated OH stretching mode with a broad adsorption in the range of 3200−3800 cm^{-1}. This observation of the HO-covered surface agreed with previous results.[31,32]

3.1. $In(CH_3)_3$ Dosage Experiment. The FTIR spectra from dosage-dependent experiments on the "clean" and HO-covered surfaces are shown in parts a and b, respectively, of Figure 1. The surfaces were exposed to $In(CH_3)_3$ for 1 min at the pressures indicated in the figures and followed by evacuation for 1 min at room temperature. The IR spectra in the two kinds of surfaces are slightly different. At low dosing pressure, $\leq$0.3 Torr, two sharp peaks appeared at ca. 2979 and 2925 cm^{-1} related to asymmetric and symmetric stretches of the methyl groups, respectively. As the dosage increased, additional two peaks at

ca. 2888 and 2822 cm^{-1} became somewhat obvious. These two peaks might be related to the C−H stretching of methyl derivatives, for example, methoxy and carboxyl groups. All the vibrations in the range of 2800−3000 cm^{-1} corresponding to the C−H stretches were originated from the adsorbed $(H_3C)_3In$ and its fragments. These results are consistent with those of TMIn on the GaAs(100) surface measured by HREELS.[23] On the HO-covered surface, the ∼3690 cm^{-1} OH stretch peak was found to be removed effectively by TMIn due to facile reaction, as will be discussed later.

These peaks were deconvoluted by four Gaussian functions. An example, the deconvolution results of a 0.5 Torr dosage spectrum on the "clean" surface, is shown in the inset of Figure 1a. The deconvoluted peak areas varying with $In(CH_3)_3$ dosing pressures are shown in Figure 1c. The solid and dotted lines are corresponding to the changes observed on the "clean" and HO-covered surfaces, respectively. Not surprisingly, all the peak areas increase as the dosage increases on both surfaces. The two peaks at 2979 and 2925 cm^{-1} with higher peak intensities and faster increasing rates than the other two peaks are related to the molecularly adsorbed $(H_3C)_3In$ and its fragments, which can easily be formed at room temperature by breaking the first In−C bond.[23,26] On the other hand, the peaks at 2888 and 2822 cm^{-1} with slower increasing rates and appearing at higher dosages on the "clean" surface are related to the CH_3 derivatives, which require higher pressures to be formed and detected. Their identities will be discussed in detail later with more information from different experiments and computational results.

The intensities of methyl vibrations are quite different on the "clean" and HO-covered surfaces at low TMIn dosages. The smaller intensities on the HO-covered surface indicates that less TMIn adsorbed on the HO-covered surface at lower dosage because a large fraction of it reacts with the HO species on the surface and eliminates its methyl as methane or methanol. The difference becomes smaller as the TMIn dosage increases because TMIn is abundant enough to saturate on these two kinds of surfaces at higher TMIn dosages.

3.2. UV Irradiation Experiments in the Absence of Oxygen. After the dosing experiments carried out at room temperature, the last samples with the highest dosages shown in parts a and b of Figure 1 were irradiated with a continuous UV lamp in the vacuum chamber to study the photolysis effect. The lamp was blocked when FTIR spectra were taken to avoid the scattered infrared from the UV source. The selected FTIR spectra of the "clean" and HO-covered surfaces with UV irradiation are shown in parts a and b, respectively, of Figure 2, and the peak areas after deconvoluting by varying with irradiation times are plotted in Figure 2c. The solid and dotted lines stand for the peak changes during the UV irradiation in the absence of O_2 on the "clean" and HO-covered surfaces, respectively.

From the figures, both surfaces show a similar trend with UV irradiation. No peak shifting or additional peaks were found in the C−H vibrational range, 2800−3000 cm^{-1}. The peaks of these methyl-related peak intensities had negligible changes during the experiments. The 2979 cm^{-1} peak was the only one decreasing and the other three peaks at 2925, 2888, and 2822 cm^{-1} slowly increased during the UV irradiation. The small changes of those IR spectra in the 2800−3000 cm^{-1} range can be explained by the UV photons breaking no chemical bonds of the adsorbates other than the weaker In−C bonds of the adsorbed $(H_3C)_3In$. The broken methyl groups with similar vibrational frequencies will remain on the surface and undergo migration forming $H_3CO(a)$ during the irradiation, similar to

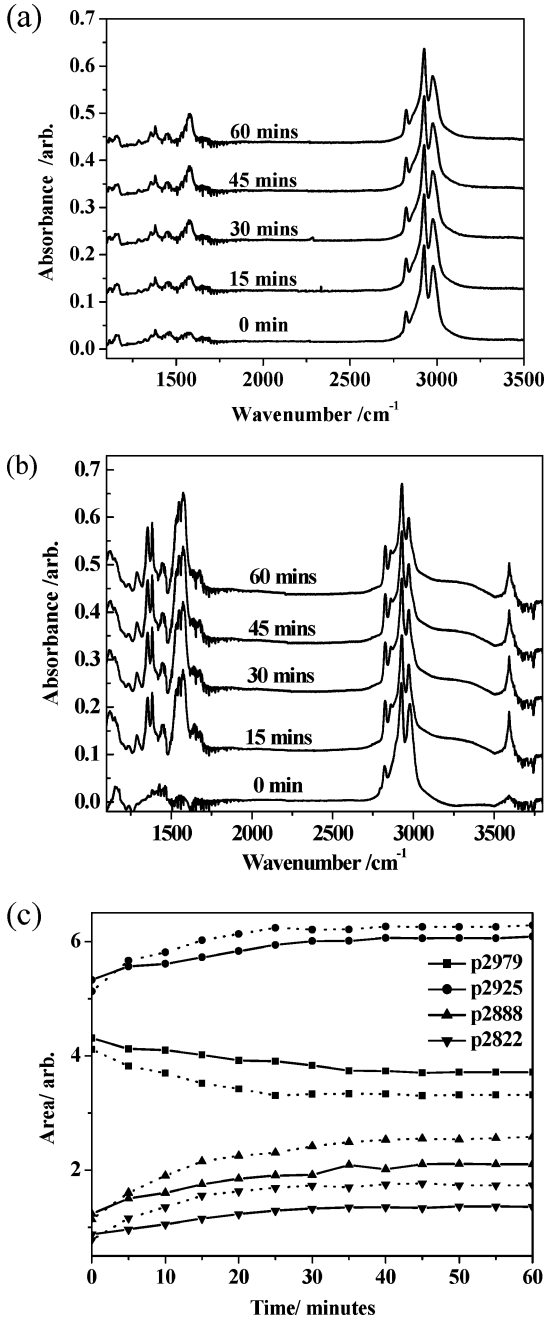

Figure 2. FTIR spectra of the UV irradiation experiment in the absence of oxygen on (a) "clean" and (b) HO-covered TiO_2 nanoparticle films. (c) Plots of peak areas as a function of UV irradiation time. Solid and dotted lines represent the changes of the "clean" and HO-covered surfaces, respectively.

the results of TMIn on the GaAs surface forming a stronger Ga−C bond.[26,27] As a result, the UV irradiation in the absence of oxygen resulted in only a small change of methyl vibrations in the FTIR spectra.

Significantly, some new peaks in the range of 1300−1600 cm^{-1} grew noticeable after the irradiation. These peaks derive primarily from the HCOO(a) species that may be formed by the oxidation of $H_3CO(a)$ with the residual amount of O_2 present in the system. These oxidation processes are more obvious if a larger amount of oxygen is present during the UV irradiation, as will be described in the following subsection.

3.3. UV Irradiation Experiment in the Presence of Oxygen. The FTIR spectra of the "clean" and HO-covered surfaces obtained in the presence of oxygen with UV irradiation

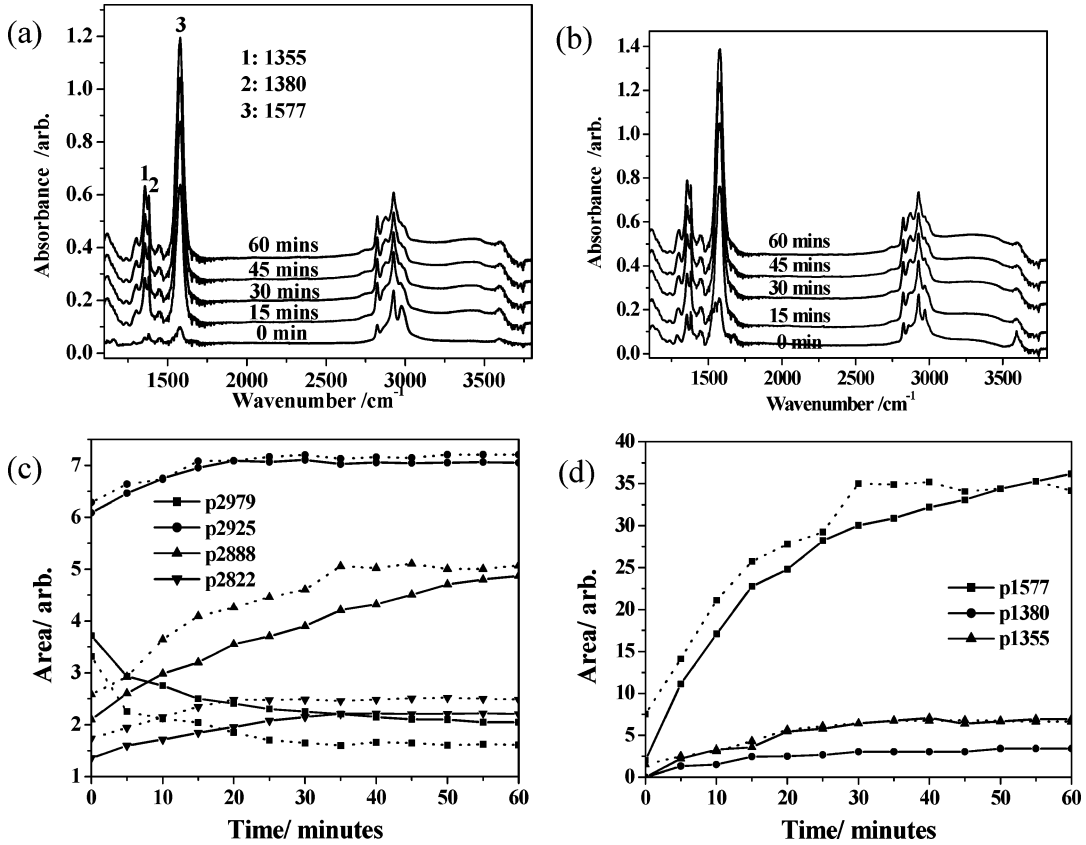

Figure 3. FTIR spectra of the UV irradiation experiment in the presence of oxygen on (a) "clean" and (b) HO-covered TiO_2 nanoparticle films. (c, d) Plots of peak areas as a function of UV irradiation time. Solid and dotted lines represent the changes of the "clean" and HO-covered surfaces, respectively.

are shown in parts a and b, respectively, of Figure 3. The four peaks related to C−H vibrations in the region of 2800−3000 cm^{-1} were noted to change dramatically, and three additional peaks at ca. 1355, 1380, and 1577 cm^{-1} grew quickly. The peak areas after deconvolution are compared in parts c and d of Figure 3. The solid and dotted lines represent the changes in the "clean" and HO-covered surfaces, respectively.

In these experiments, the strong oxidant can be formed by UV irradiation in the presence of oxygen with TiO_2:[33]

$$TiO_2 + UV \rightarrow e^- + h^+$$

$$e^- + O_2 \rightarrow O_2^-$$

These processes are related to the high photocatalytic ability of TiO_2 which has been widely applied in waste treatments.[34,35] The strong O_2^- oxidant is able to convert the $H_3CO(a)$ to $HCOO(a)$[36−39] and thus explains the changes in the FTIR spectra. In the first step, more methyl groups attached to the In atom are oxidized to $H_3CO(a)$. In this process, the H_3C-related peak at 2979 cm^{-1} dropped rapidly as the H_3CO-related peak at 2822 cm^{-1} increased. The peak at 2925 cm^{-1} originated from both H_3C groups and $H_3CO(a)$ remained constant after the initial small increase. The increasing rate of the $H_3CO(a)$ peak at 2822 cm^{-1} was small because, in the ensuing step, $H_3CO(a)$ could be further oxidized to form HCOO(a), whose related four peaks, υ_s(CH) at 2888 cm^{-1}, υ_a(OCO) at 1577 cm^{-1}, δ(CH) at 1380 cm^{-1}, and υ_s(OCO) at 1355 cm^{-1},[36,40] were found to increase rapidly during the entire experiments. The fact that the increasing rates of these peaks are different can be attributed to the different IR intensities. However, the similar trend among them implies that these peaks are related to the same species. In addition, these vibrational frequency assignments can be confirmed by first-principles calculations in section 5.3, and the series of oxidation processes are consistent with similar photooxidation results of dimethylmethylphosphonate,[36] methanol,[37] ethanol,[38] and methylamine[39] on powdered TiO_2 nanoparticle films.

3.4. Surface Annealing Experiment. After 60 min of UV irradiation in the presence of oxygen, the last samples shown in parts a and b of Figure 3 were annealed at different temperatures to study the thermal effect. The surfaces were cooled from the indicated temperatures to room temperature when the spectra were taken to avoid excited phonon emissions. The FTIR spectra of the "clean" and HO-covered surfaces with annealing are shown in parts a and b, respectively, of Figure 4. Varying with surface temperatures, the peak areas after deconvoluting are shown in parts c and d of Figure 4. The solid and dotted lines symbolize the changes in the "clean" and HO-covered surfaces, respectively.

In this annealing experiment, all the peaks decreased as the surface temperatures increased, and these peaks disappeared completely when the surfaces were annealed up to 523 K. The H_3C-related peak at 2979 cm^{-1} diminished quickly from 398 to 448 K; the $H_3CO(a)$-related peak at 2822 cm^{-1} dropped swiftly from 423 to 473 K; similarly, the HCOO(a)-related peaks at 2888, 1577, 1380, and 1355 cm^{-1} also vanished from 423 to 448 K. The decreasing rates of these adsorbates show no significant differences.

To conclude the experimental results, as aforementioned, the peaks at 2979 and 2925 cm^{-1} are attributable to the asymmetric and symmetric vibrations of the methyl groups in the molecularly adsorbed TMIn and its fragments on the surface. During UV irradiation in the absence of oxygen, the 2979 cm^{-1} peak deceases somewhat with irradiation time with a concomitant

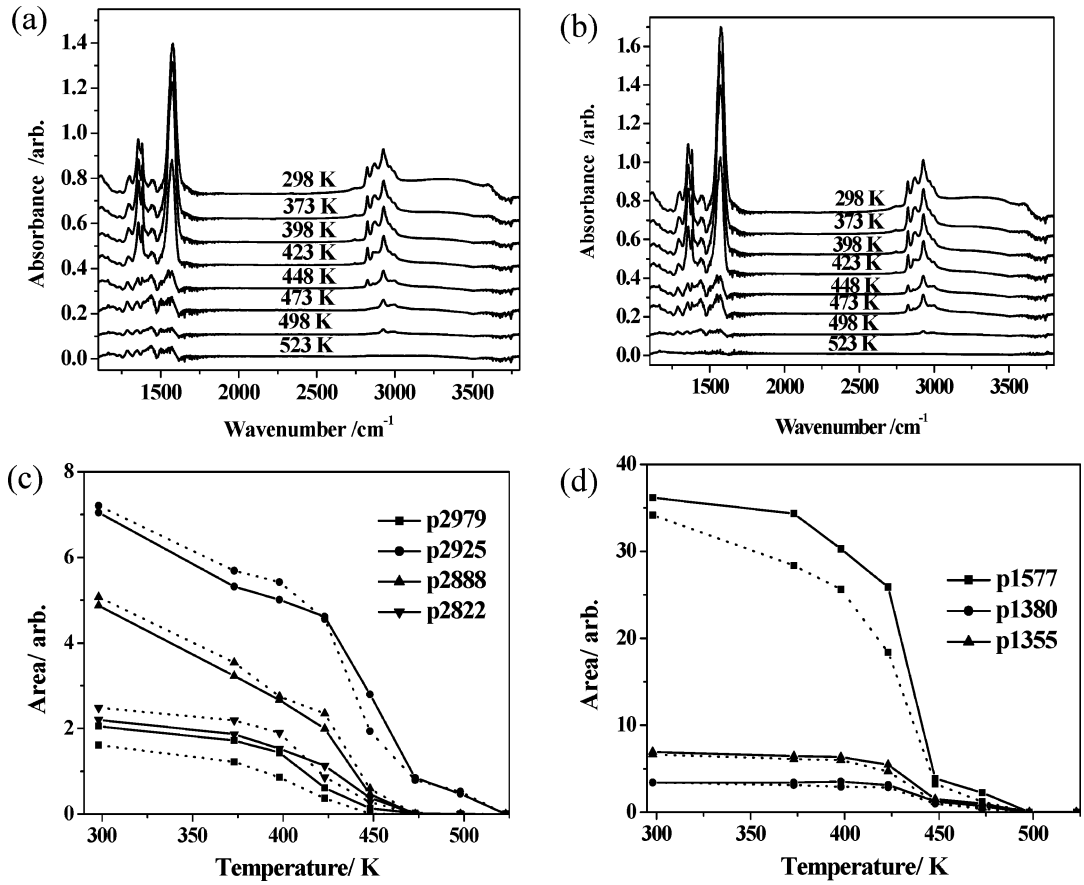

Figure 4. FTIR spectra of the surface annealing experiment on (a) "clean" and (b) HO-covered TiO_2 nanoparticle films. (c, d) Plots of peak areas as a function of annealed temperature. Solid and dotted lines represent the changes of the "clean" and HO-covered surfaces, respectively.

small increase of the 2925 and 2822 cm^{-1} peaks attributable to the formation of CH_3O(a). Overall, the FTIR spectra showed limited changes. On the other hand, with UV irradiation in the presence of oxygen, the adsorbates could be oxidized from CH_3 attached to the In atom to CH_3CO to HCOO by the strong oxidant, O_2^-. The spectra showed dramatic changes with this trend. Finally, in the surface annealing experiments, all these peak intensities dropped as the surface temperatures increased and totally disappeared at 523 K.

It is worth noting that no significant differences were found between the "clean" and HO-covered surfaces. This can be rationalized by the fact that TiO_2 nanoparticles easily retain OH groups on their surfaces.[41,42] Even treated with high temperature heating in a vacuum, the OH groups still remain on TiO_2 nanoparticle surfaces. Since the "clean" surface spectrum was used as background, these "hidden" OH groups on the "clean" surface could not be detected in Figure 1a. On the other hand, the OH vibrations on the HO-covered surfaces in Figure 1b could be attributed to the highly saturated OH groups, which can be consumed by TMIn immediately as described above.

Current experimental results are similar to the experimental results of TMIn on other semiconductor surfaces,[23,36,39] but no energetic detail had been discussed in detail to date. In the next two sections, the mechanism of surface reactions will be elucidated by first-principles calculations and comparison with current experimental data will also be made.

4. Computational Method

The geometric structures and related energies were optimized and calculated by the Vienna Ab initio Simulation Package (VASP),[43−46] implementing the density functional theory (DFT) with local-density approximation (LDA).[47] The Perdew−Wang 1991 (PW91) formulation,[48] which worked well for surfaces,[49] was used in the generalized gradient approximation (GGA)[48,50] for the total energy calculations. The pseudopotentials supplied with VASP were applied to the core electrons. The 10 valence electrons, $3p$,[6] $4s^2$, and $3d^2$, of each Ti atom and the six valence electrons, $2s^2$ and $2p^4$, of each O atom were explicitly considered in the calculation. Their orbitals were expanded in a plane-wave basis for the periodic properties and all plane waves with kinetic energies smaller than the chosen cutoff energy for the basis set convergence.

As reasoned and completely described in our previous work,[8] the TiO_2(110) surface, modeled as an infinite slab, was employed for simulating the film of TiO_2 nanoparticles. Briefly, a supercell, consisting of 16 [TiO_2] units with the bond lengths and angles initially defined according to the experimental value,[51] extended periodically in three directions: repetition in the plane creates an infinite slab, and periodicity in the direction perpendicular to the slab creates an infinite stack of slabs. This surface supercell has dimensions of $\sqrt{2}a \times c$ along the $(\bar{1}10)$ and (001) directions, where a and c are the lattice constants of the bulk TiO_2 unit cell, and contains four layers of the (110) plane with the bridged oxygen and titanium atoms on top of the surface as active sites. This generates an infinite stack of quasi-two-dimensional slabs, each separated from its neighbors by a certain vacuum layer. To minimize the interaction between distinct slab surfaces in this infinitely periodic model system, the vacuum separation on top is chosen equal to 10.4 Å, which is the same as previous studies.[8] A 600 eV cutoff energy and $4 \times 5 \times 1$ Monkhorst−Pack k-points[52] were employed in the current calculation. The first layer in the bottom was fixed to

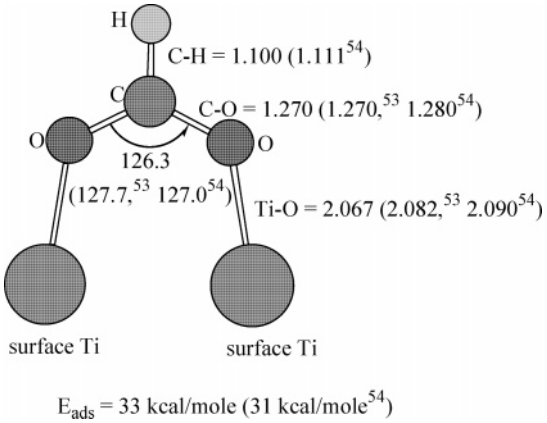

Figure 5. Adsorption energy and optimized structures of adsorbed HCOO(a) on two surface Ti atoms compared with previous results[53,54] in parentheses.

ensure no substantial interactions between the neighboring slabs. All these parameters were applied successfully to the HN_3/TiO_2 system[8] and provided a good description of gas−surface reactions.

Furthermore, the reliability of this model was tested by computing the adsorption of the carboxyl group on the surface, which was observed from the UV irradiation experiment in the presence of oxygen discussed in section 3.3. The most stable adsorption structure, α-OC(H)O(a), has two oxygen atoms of the carboxyl group bonded to two surface Ti atoms, as shown in Figure 5. Comparing the adsorption energy and geometric structure of this species, the current computed results show close agreement with previous values,[53,54] implying that these parameters can be reliably applied to the current $TMIn/TiO_2$ system.

As described in the HN_3/TiO_2 system,[8] a two-layer TiO_2 cluster has been shown to be sufficient for simulating the force field of the TiO_2 surface affecting the adsorbate vibrations. Therefore, the vibrational frequencies were modeled by the optimized structures in the slab model calculation with two layers of TiO_2 (eight [TiO_2] units) and calculated by a hybrid Hartree−Fock/density functional theory (HF/DFT) method, B3LPY, which includes Becke's three-parameter nonlocal-exchange function[55] with the correlation functional of Lee−Yang−Parr,[56] and the standard all-electron split-valence basis set 6-31G(d)[57] in Gaussian03.[58]

5. Computational Results and Discussion

To elucidate the experimental results, the surface reactions of TMIn on TiO_2 have been computed in detail. Since the oxidation process from the adsorbed methyl groups to the carboxyl group, which is related to the experiment of UV irradiation in the presence of oxygen, had been studied extensively,[36,38,39] the oxidization processes were not computed and discussed here. Three major reactions, including the methyl group elimination, the methane elimination, and the methyl group migration processes, have been comprehensively investigated in this computational section.

As shown in the computed potential energy surface of TMIn on "bare" TiO_2 surface in Figure 6, two reactions can occur on the surface via $(H_3C)_3In-O_b(a)$: one produces $(H_3C)_2In-O_b(a) + H_3C(a)$, where one of the CH_3 groups is dissociatively adsorbed on a bare Ti atom ("O_b" stands for the bridged oxygen). The reaction is exothermic by 10 kcal/mol with a 23 kcal/mol activation barrier forming $(H_3C)_2In-O_b(a)$. The other path, $(H_3C)_3In-O_b(a) \rightarrow (H_3C)_2In-O_b(a) + H_3C-O_b(a)$, which

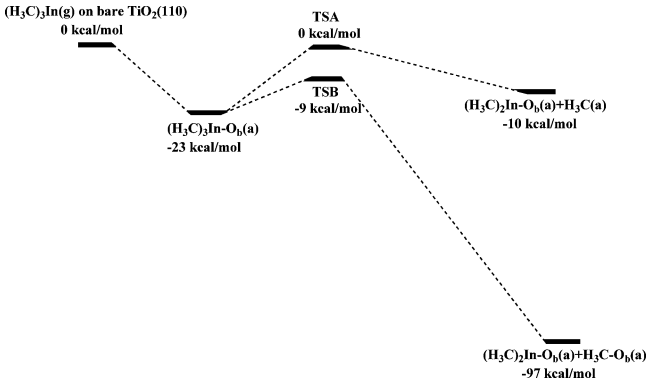

Figure 6. Surface reactions of TMIn on bare $TiO_2(110)$ surface.

takes place via a small 4 kcal/mol barrier, is more exothermic, −97 kcal/mol. Contrary to the strong binding at the O_b site, the CH_3 can only bond weakly with surface Ti atoms, and the indium and indium-containing species cannot bond with the surface Ti atoms since both indium and titanium are electron-deficient metal atoms. Furthermore, the experimental results from both "clean" and HO-covered surfaces were quite similar, which is related to the fact that powdered TiO_2 films have been proven to retain OH groups on the surface, even at high temperatures in a vacuum as mentioned above.[41,42]

Reasoned from the above, the reactions on the HO-covered TiO_2 surface are discussed in detail here. The results of geometric optimization and adsorption energies of possible adsorbed species are presented in section 5.1. To account for the experimental observations, the potential energy surfaces of reactions are plotted by calculating the key transition states in section 5.2. Finally, the computed frequencies of these stable species are compared with the experimental results in section 5.3.

5.1. Adsorbate Structures and Adsorption Energies. The possible surface species, $(CH_3)_3In$ and its fragments, including $(CH_3)_2In$, CH_3In, CH_3, and In, adsorbing on the surface active sites, the bridged oxygen (O_b), and the oxygen atom of the OH group covering the surface, were computed by the VASP code. The optimized structures with the partial surface model for brevity are shown in Figure 7. The selected bond lengths, CH-related vibrations calculated at the B3LYP/6-31G(d) level (with the scaling factor,[59] 0.98), and adsorption energies of these optimized adsorbates are listed in Table 1.

For the C−H bonds in all the adsorbates, the maximum difference in bond length is less than 0.01 Å. For indium-related bonds, the In−O_b or In−O bond lengths exhibit a slightly increasing trend following the order of $(H_3C)_3In(a) < (H_3C)_2In(a) < H_3CIn(a) < In(a)$, and the In−C bond lengths show a reverse trend (see Table 1). However, these differences in the bond lengths provide limited information on their stabilities.

The $(H_3C)_2In$ adsorbates, $(H_3C)_2In-O_b(a)$, $(H_3C)_2In-O(H)(a)$, and $(H_3C)_2In-O(a)$, are more stable than their related $(H_3C)_3In$ or H_3CIn adsorbates, $(H_3C)_3In-O_b(a)$, $(H_3C)_3In-O(H)(a)$, and $(H_3C)_3In-O(a)$ or $H_3CIn-O_b(a)$, $H_3CIn-O(H)(a)$, and $H_3CIn-O(a)$. The stable $(H_3C)_2In$ adsorbates indicate that indium, an element in group III, is favored to be 3-fold coordinated. Comparing the three $(H_3C)_2In$ species adsorbing on the different surface sites of O_b, OH, and O, $(H_3C)_2In-O(a)$ is most stable with 92 kcal/mol adsorption energy. This can also be explained by the most stable 2-fold-coordinated oxygen atom in $(H_3C)_2In-O(a)$. The other oxygen atoms of the surface O_b and OH sites are 3-fold coordinated when they are bonded with adsorbates and are less stable. Therefore, the adsorption energy of an In-related adsorbate adsorbed on surface O site is

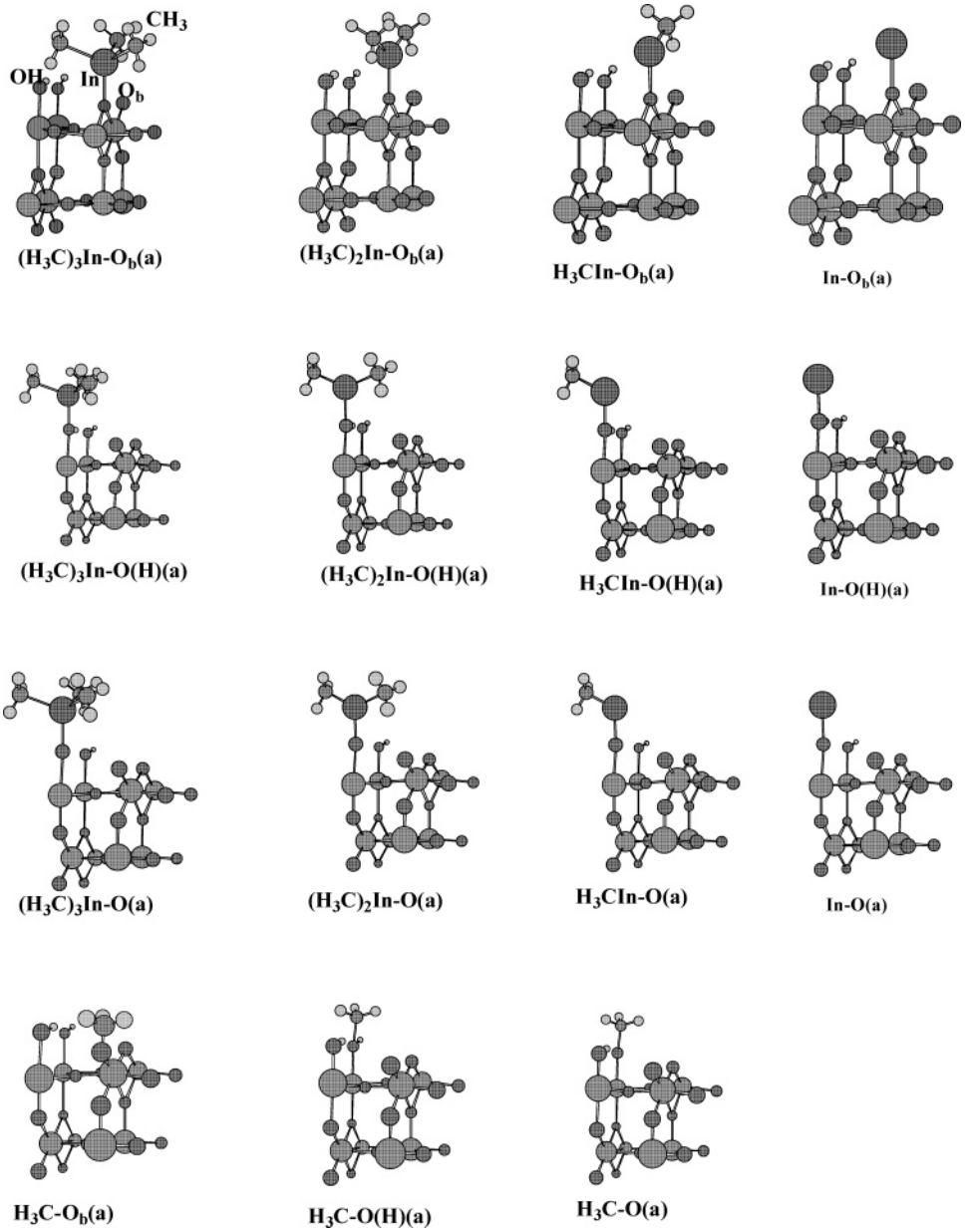

Figure 7. Optimized structures of possible adsorbates listed in Table 1 displayed with two layers of the TiO_2(110) surface model for brevity.

higher than that adsorbed on surface O_b and HO sites (Table 1). The results imply that a hydroxylated clean TiO_2 surface can enhance the adsorption of In-containing species.

5.2. Surface Reactions and PES. Since the current surface model contained two surface Ti atoms, which were both covered with HO(a) groups, the initial reactants included two adsorbed HO(a) groups and one unreacted $(H_3C)_3In(g)$ in the gas phase, $(H_3C)_3In(g) + 2HO(a)$. Starting with $(H_3C)_3In$ molecularly adsorbed on the surface forming $(H_3C)_3In-O_b(a) + 2HO(a)$ and $(H_3C)_3In-O(H)(a) + HO(a)$, as shown in Figures 8 and 9, respectively, three types of the surface reactions, CH_3 elimination, CH_3 migration, and CH_4 elimination, were computed. All the elimination reactions are endothermic processes, and the migration reactions are exothermic processes.

CH_3 elimination is a direct dissociation process by breaking either In−C or O−C bonds without intrinsic barriers. Based on the results in Figures 8 and 9, the methyl group forms a weaker bond with metal In, ∼27 kcal/mol. (It also forms a weaker bond with a surface metal Ti atom, 13 kcal/mol, in Figure 6.) On the other hand, the bonds between the methyl group and surface oxygen are much stronger: H_3C-O_b, 100 kcal/mol, and $H_3C-O(H)$, 102 kcal/mol (see Table 1). Therefore, the methyl group can bond with the surface oxygen tightly but dissociate from the adsorbed TMIn easily. These results also can explain the CH_3 migration process in the following.

The CH_3 migration results from two concurrent processes: CH_3 elimination from an adsorbed TMIn and CH_3 adsorption on an O_b or O atom of the surface OH group. As described above, the highly exothermic adsorption energy of the methyl group and less endothermic energy of CH_3 elimination make the heat of reaction in CH_3 dissociative adsorption (or the migration from the In to an O atom) to be highly exothermic. Furthermore, the transition states, TS2, TS3, TS6, and TS7, in the CH_3 migration processes are energetically lower than the initial reactants, $(H_3C)_3In(g) + 2HO(a)$, and their barriers are also smaller, 11−18 kcal/mol. The lower barriers of these transition states are related to their structures, in which the weaker In−C bonds are lengthened while the stronger O−C bonds are shortened, in the middle of reactants and products. Therefore, this result is consistent with our experimental observation that the IR intensities of methyl peaks changed slightly in the UV irradiation in the absence of oxygen

TABLE 1: Selected Bond Lengths (Å), CH Related Vibrational Frequencies, and Adsorption Energies[a] (kcal/mol) of Various Adsorbates Predicted by Calculations

	In−O_b or C−O_b	In−O or C−O	In−C	C−H	υ_a(CH)[a]	υ_s(CH)[a]	E_{ads}[b]
$(H_3C)_3In-O_b(a)$	2.064		2.283	1.091	2988	2920	23
$(H_3C)_2In-O_b(a)$	2.095		2.206	1.090	2978	2910	74
$H_3CIn-O_b(a)$	2.115		2.150	1.094	2985	2911	63
$In-O_b(a)$	2.138						102
$(H_3C)_3In-O(H)(a)$		2.079	2.213	1.092	2979	2936	19
$(H_3C)_2In-O(H)(a)$		2.097	2.197	1.095	2979	2926	69
$H_3CIn-O(H)(a)$		2.150	2.101	1.090	2975	2930	61
$In-O(H)(a)$		2.195					94
$(H_3C)_3In-O(a)$		2.000	2.198	1.094	2987	2934	43
$(H_3C)_2In-O(a)$		2.017	2.173	1.093	2983	2930	92
$H_3CIn-O(a)$		2.073	2.140	1.090	2985	2930	78
$In-O(a)$		2.133					115
$H_3C-O_b(a)$	1.423			1.096	2987	2934	100
$H_3C-O(H)(a)$		1.439		1.092	2946	2855	102
$H_3C-O(a)$		1.394			2928	2827	118

[a] Present experimental values for H_3C stretches are 2979 and 2925 cm^{-1}; those for H_3CO stretches are 2925 and 2822 cm^{-1}. [b] $E_{ads} = -(E_{total} - E_{molecule} - E_{surface})$, for TMIn and its fragments on HO-covered TiO_2(110) surface predicted with the slab model using VASP. The related structures are shown in Figure 7.

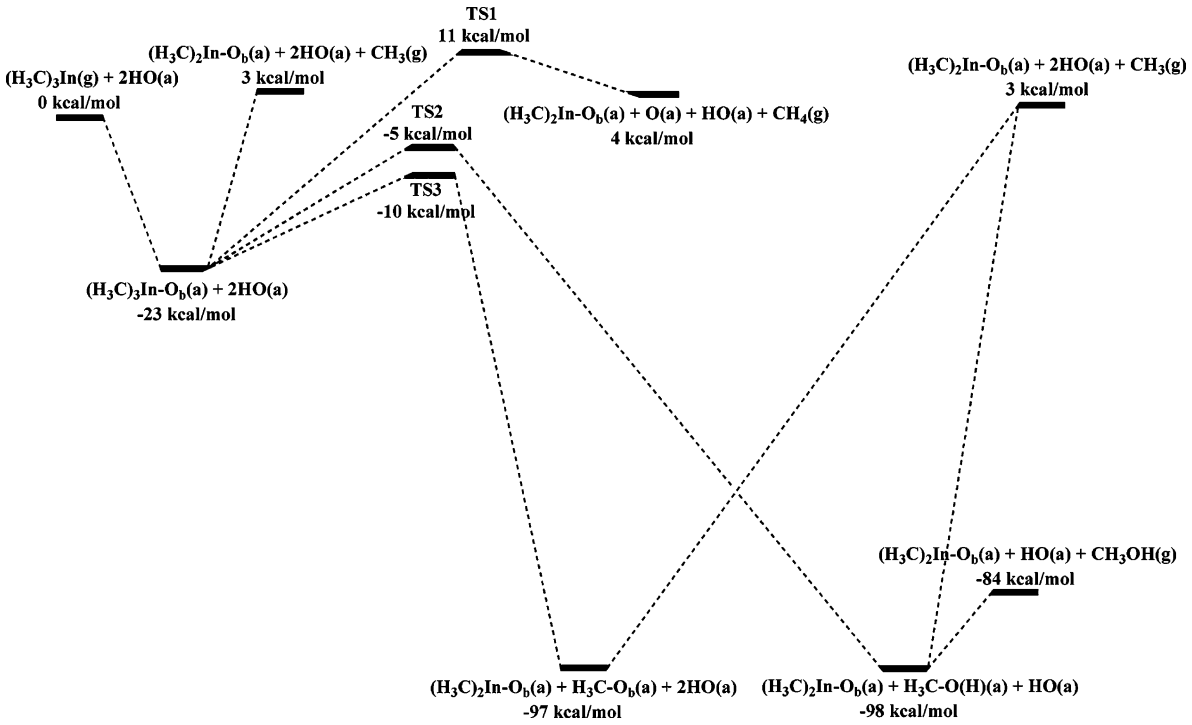

Figure 8. Potential energy surface related to surface reactions starting from $(H_3C)_3In$ adsorbed on the bridged oxygen, $(H_3C)_3In-O_b(a)$.

experiments because the methyl group can migrate and remain on the surface with external energy provided by heating or UV irradiation at room temperature.[26,27]

Finally, CH_4 elimination can be considered as the combination of three processes: CH_3 elimination, O−H bond breaking, and C−H bond formation. The energy required for the O−H bond breaking process is similar to the energy released from the C−H bond formation. Therefore, CH_4 elimination has an endothermicity similar to that of the CH_3 elimination process. Unlike CH_3 migration, the CH_4 elimination processes are less favored to happen on the surface because the transition states, TS1, TS4, and TS5, are energetically higher than the initial reactants and their barriers are over 31 kcal/mol. These energetically higher transition states are related to the breaking of the strong O−H bonds.

5.3. Vibrational Frequency Analysis. The geometric structures and related strong antisymmetric stretch and symmetric stretch vibrations of of CH_3, υ_a(CH) and υ_s(CH), are shown in Figure 7 and Table 1, respectively. The four strong peaks related to CH_3 vibrations in the 2800−3000 cm^{-1} range can be resolved by computational analysis. The adsorbed species, $(H_3C)_3In-O_b(a)$, $(H_3C)_2In-O_b(a)$, $H_3CIn-O_b(a)$, $H_3C-O_b(a)$, $(H_3C)_3In-O(H)(a)$, $(H_3C)_2In-O(H)(a)$, $H_3CIn-O(H)(a)$, $(H_3C)_3In-O(a)$, $(H_3C)_2In-O(a)$, and $H_3CIn-O(a)$, all have close υ_a(CH) and υ_s(CH) in the ranges of 2998−2975 and 2910−2936 cm^{-1}, which may be compared with current experimental results, 2979 and 2925 cm^{-1}, respectively. The better agreement of the predicted $(H_3C)_2In-O_b(a)$ vibrations than those of $(H_3C)_3In-O_b(a)$ with the experimental values indicates that $(H_3C)_2In-O_b(a)$ is more stable and may be formed directly by dissociative adsorption as explained in section 5.1.

On the other hand, the CH_3 stretches of the methoxy adsorbates, $H_3C-O(H)(a)$ and $H_3C-O(a)$, are different from those of the aforementioned species. The experimental values with υ_a(CH) = 2925 cm^{-1} and υ_s(CH) = 2822 cm^{-1} are closely related to the vibrations of $H_3C-O(a)$ with υ_a(CH) = 2928 and

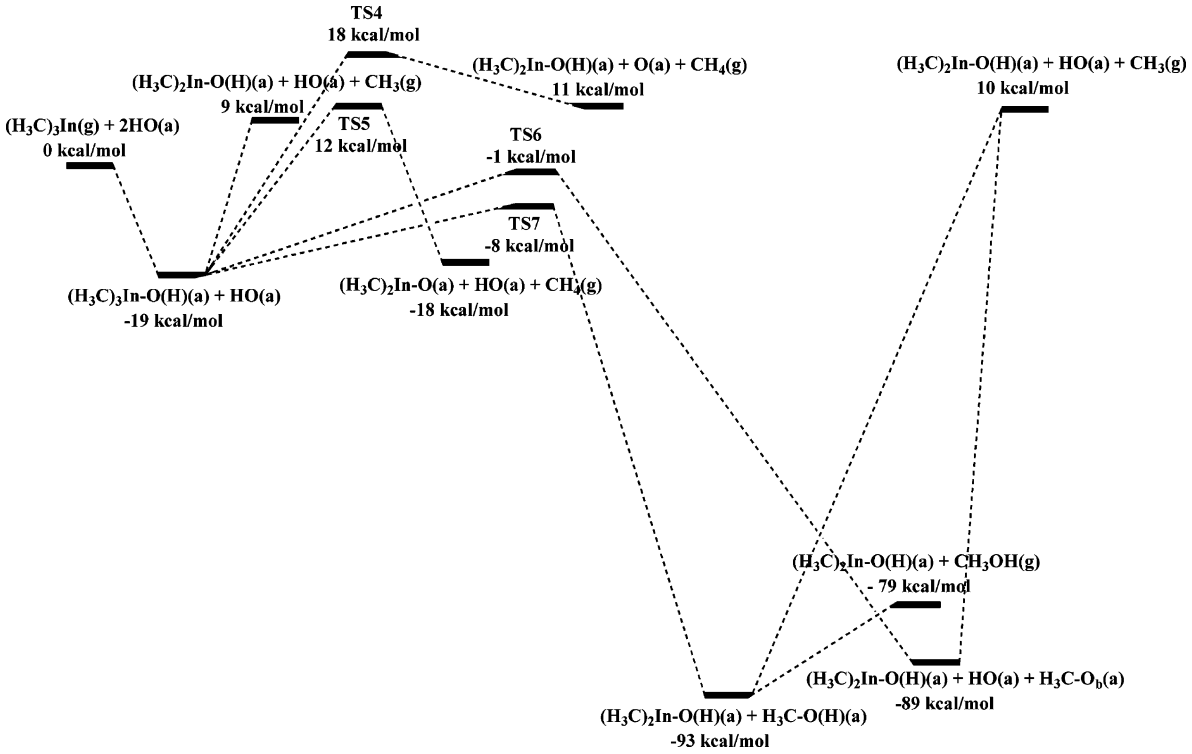

Figure 9. Potential energy surface related to surface reactions starting from $(H_3C)_3In$ adsorbed on the oxygen of the HO group, $(H_3C)_3In-O(H)(a)$.

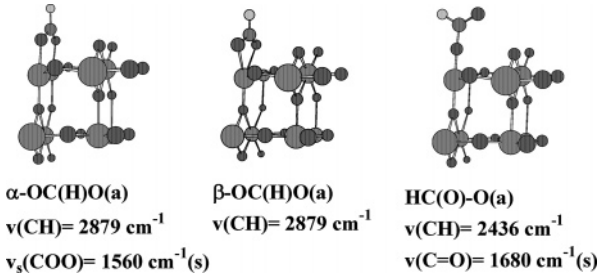

Figure 10. Geometric structures and related vibrational frequencies of possible HCOO adsorption structures. Comparison with FTIR observations of $\nu(CH) = 2888\ cm^{-1}$ and $\nu_a(OCO) = 1577\ cm^{-1}$.

$\nu_s(CH) = 2827\ cm^{-1}$ rather than the vibrations of $H_3C-O(H)$-(a) with $\nu_a(CH) = 2946\ cm^{-1}$ and $\nu_s(CH) = 2855\ cm^{-1}$. This is because the weakly adsorbed methanol is easily desorbed from the surface. It is worth noting that the computed 20 cm^{-1} vibrational shifting between methoxy and methanol adsorbates also agrees well with previous experimental observations.[37,41]

In addition, the ν_s(OCO) vibrations of the three possible structures, α-OC(H)O(a), *β*-OC(H)O(a), and HC(O)O(a), of the adsorbed HCOO(a) generated from the oxidation process in the UV irradiation experiment in the presence of O_2 are also computed, as shown in Figure 10. In the computed HC(O)O(a) structure, there is a strong C═O vibration (∼1680 cm^{-1}) which was not observed in the FTIR spectra. The computed *β*-OC-(H)O(a) does not exhibit a strong ν_a(OCO) vibration. On the other hand, the FTIR observed HCOO(a) frequencies agree well with predicted frequencies of α-OC(H)O(a). This prediction is also consistent with previous experimental works.[36,40] Furthermore, the experimentally observed structure α-OC(H)O(a) has two oxygens doubly bonded on the surface, which makes α-OC-(H)O(a) the most stable structure with $E_{ads} = 33$ kcal/mol.

6. Summary

In this work, the adsorption and reactions of TMIn on TiO_2 nanoparticle films have been experimentally studied by FTIR spectroscopy, monitoring the effects of dosage, UV irradiation in both the absence and presence of oxygen, and surface annealing. Computationally, the adsorption energies and vibrational frequencies of the possible adsorbates have been predicted by first-principles calculations.

In the dosage and UV irradiation experiments in the absence of oxygen, the CH_3 vibrations derive mainly from the adsorbed TMIn and its derivatives including $CH_3O(a)$. Some of the methyl groups attached to the In atom can migrate onto the surface at room temperature or by UV photons. Therefore, the FTIR spectra revealed only minor changes in these experiments. This interpretation is consistent with the computed potential energy surfaces in Figures 8 and 9, which show that CH_3 migration has low transition state barriers and is highly exothermic because of the weak $In-CH_3$ and strong H_3C-O_b or $H_3C-O(H)$ bonds.

On the other hand, in the UV irradiation in the presence of oxygen, more methyls can be oxidized to methoxy and to the carboxyl, which is substantiated by its adsorption peaks at 1577, 1380, and 1355 cm^{-1}. The computed results further confirmed the structure of the adsorbed carboxyl on TiO_2 surface as α-OC-(H)O(a). The adsorption energies of several adsorbates on O_b atoms and the HO-covered Ti atoms have been computed.

Acknowledgment. J.-H.W. is grateful for the support from the Graduate School of Emory University for this study, and M.C.L. acknowledges the support from the R.W. Woodruff Professorship at Emory University and from Taiwan's National Science Council for a Distinguished Visiting Professorship at the Center for Interdisciplinary Molecular Science, National Chiao Tung University, Hsinchu, Taiwan. The authors are also grateful to the Cherry L. Emerson Center of Emory University, which is in part supported by a National Science Foundation grant (CHE-0079627) and an IBM shared University Research Award, and the National Center for High-Performance Computing in Taiwan for the use of their resources. The authors also thank Dr. Wei, C. M. in Academia Sinica, Taiwan, and Dr. Sun in National Taiwan Normal University for VASP calculations

and Dr. Lian, Tim, and his group in Emory University for instruction in the preparation of TiO_2 nanoparticle films.

References and Notes

(1) Irie, H.; Watanabe, Y.; Hashimoto, K. *J. Phys. Chem. B* **2003**, *107*, 5483.
(2) Asahi, R.; Morikawa, T.; Ohwaki, T.; Aoki, K.; Taga, Y. *Science* **2001**, *293*, 269.
(3) Burda, C.; Lou, Y.; Chen, X.; Samia, A. C. S.; Stout, J.; Gole, J. L. *Nano Lett.* **2003**, *3*, 1049.
(4) Gratzel, M. *Nature* **2001**, *414*, 338.
(5) Nedeljkovic, J. M.; Micic, O. L.; Ahrenkiel, P.; Miedaner, A.; Nozik, A. J. *J. Am. Chem. Soc.* **2004**, *126*, 2632.
(6) Wang, J.-H.; Lin, M. C. *ChemPhysChem* **2004**, *5*, 1615.
(7) Nazeeruddin, M.-K.; Kay, A.; Rodicio, I.; Humphry-Baker, R.; Muller, E.; Liska, P.; Vlachopoulos, N.; Gratzel, M. *J. Am. Chem. Soc.* **1993**, *115*, 6328.
(8) Wang, J.-H.; Lin, M. C.; Sun, Y. C. In press.
(9) Xu, K.; Yoshikawa, A. *Appl. Phys. Lett.* **2003**, *83*, 251.
(10) Matsuoka, T.; Okamoto, H.; Nakao, M.; Harima, H.; Kurimoto, E. *Appl. Phys. Lett.* **2002**, *81*, 1246.
(11) Bu, Y.; Ma, L.; Lin, M. C. *J. Vac. Sci. Technol., A* **1993**, *11*, 2931.
(12) Yang, F.-H.; Hwang, J.-S.; Chen, K.-H.; Yang, Y.-J.; Lee, T.-H.; Hwa, L.-G.; Chen, L.-C. *Thin Solid Films* **2002**, *405*, 194.
(13) Lu, H.; Schaff, W. J.; Eastman, L. F. *J. Appl. Phys.* **2004**, *96*, 3577.
(14) Yamamoto, A.; Tsujino, M.; Ohkubo, M.; Hashimoto, A. *Sol. Energy Mater. Sol. Cells* **1994**, *35*, 53.
(15) Wang, Y.; Hwang, G. S. *Surf. Sci.* **2004**, *385*, 144.
(16) Feng, S.-W.; Tang, T.-Y.; Lu, Y.-C.; Liu, S.-J.; Lin, E.-C.; Yang, C. C.; Ma, K.-J.; Shen, C.-H.; Chen, L. C.; Kim, K. H.; Lin, J. Y.; Jiang, H. X. *J. Appl. Phys.* **2004**, *95*, 5388.
(17) Johnson, N. M.; Nurmikko, A. V.; DenBaars, S. P. *Phys. Today* **2000**, *53*, 31.
(18) Nakamura, S.; Senoh, M.; Nagahama, S.-I.; Iwasa, N.; Matsushita, T.; Mukai, T. *Appl. Phys. Lett.* **2000**, *76*, 22.
(19) Schumann, O.; Geelhaar, L.; Riechert, H.; Cerva, H.; Abstreiter, G. *J. Appl. Phys.* **2004**, *96*, 2832.
(20) Zaban, A.; Micic, O. I.; Gregg, B. A.; Nozik, A. J. *Langmuir* **1998**, *14*, 3153.
(21) Horwitz, J. S.; Villa, E.; Hsu, D. S. Y. *J. Phys. Chem.* **1990**, *94*, 7214.
(22) Villa, E.; Horwitz, J. S.; Hsu, D. S. Y. *Chem. Phys. Lett.* **1989**, *164*, 587.
(23) Aquino, A. A.; Mulcahy, C. P. A.; Jones, T. S. *Surf. Sci.* **1995**, *344*, L1231.
(24) Aquino, A. A.; Mulcahy, C. P. A.; Jones, T. S. *Chem. Phys. Lett.* **1996**, *252*, 159.
(25) Donnelly, V. M.; McCaulley, J. A. *Surf. Sci.* **1990**, *235*, L333.
(26) Shogen, S.; Ohashi, M.; Hashimoto, S.; Kawasaki, M.; Hosokawa, Y. *Mater. Res. Soc. Symp. Proc.* **1993**, *280*, 193.
(27) Shogen, S.; Matsumi, Y.; Kawasaki, M. *Thin Solid Films* **1992**, *218*, 58.
(28) Bu, Y.; Chu, J. C. S.; Lin, M. C. *Mater. Lett.* **1992**, *14*, 207.
(29) Zaban, A.; Ferrere, S.; Sprague, J.; Gregg, B. A. *J. Phys. Chem. B* **1997**, *101*, 55.
(30) Basu, P.; Ballinger, T. H.; Yates, Jr., J. T. *Rev. Sci. Instrum.* **1988**, *59*, 1321.
(31) Lewis, K. E.; Parfitt, G. D. *Trans. Faraday Soc.* **1966**, *62*, 204.
(32) Jackson, P.; Parfitt, G. D. *Trans. Faraday Soc.* **1971**, *67*, 2469.
(33) Egerton, T. A.; Tooley, I. R. *J. Phys. Chem. B* **2004**, *108*, 5066.
(34) Fujisjima, A.; Hashaimoto, K.; Watanabe, T. *TiO_2 Photocatalysis: Fundamentals and Applications*; Bkc, Inc.: Tokyo, 1999.
(35) Ollis, D.; El-Akabi, H. *Photocatalytic Purification and Treatment of Water and Air*; Elsevier: New York, 1993.
(36) Rusu, C. N.; Yates, J. T., Jr. *J. Phys. Chem. B* **2000**, *104*, 12299.
(37) Chuang, C.-C.; Chen, C.-C.; Lin, J.-L. *J. Phys. Chem. B* **1999**, *103*, 2439.
(38) Wu, W.-C.; Chuang, C.-C.; Lin, J.-L. *J. Phys. Chem. B* **2000**, *104*, 8719.
(39) Liao, L.-F.; Wu, W.-C.; Chuang, C.-C.; Lin, J.-L. *J. Phys. Chem. B* **2001**, *105*, 5928.
(40) Rotzinger, F. P.; Kesselman-Truttmann, J. M.; Hug, S. J.; Shklover, V.; Graetzel, M. *J. Phys. Chem. B* **2004**, *108*, 5004.
(41) Taylor, E. A.; Griffin, G. L. *J. Phys. Chem.* **1988**, *92*, 477.
(42) Hussein, G. A. M.; Sheppard, N.; Zaki, M. I.; Fahim, R. B. *J. Chem. Soc., Faraday Trans. 1* **1991**, *87*, 2655.
(43) Kresse, G.; Hafner, J. *Phys. Rev. B* **1993**, *47*, 558.
(44) Kresse, G.; Hafner, J. *Phys. Rev. B* **1994**, *49*, 14251.
(45) Kresse, G.; Furthmuller, J. *Comput. Mater. Sci.* **1996**, *6*, 15.
(46) Kresse, G.; Furthmuller, J. *Phys. Rev. B* **1996**, *54*, 11169.
(47) Cleperley, D. M.; Alder, B. J. *Phys. Rev. Lett.* **1980**, *45*, 566.
(48) Perdew, J. P.; Yang, Y. *Phys. Rev. B* **1992**, *45*, 244.
(49) Perdew, J. P.; Chevary, J. A.; Vosko, S. H.; Jackson, K. A.; Penderson, M. R.; Singh, D. J.; Fiolhais, C. *Phys. Rev. B* **1992**, *46*, 6671.
(50) Lee, C.; Yang, W.; Parr, R. G. *Phys. Rev. B* **1988**, *37*, 785.
(51) Wyckoff, R. W. G. *Crystal Structure*, 2nd ed.; Wiley: New York, 1964; Vol. 1.
(52) Monkhorst, H.; Pack, J. *Phys. Rev. B* **1976**, *13*, 5188.
(53) Sayago, D. I.; Polcik, M.; Lindsay, R.; Toomes, R. L.; Hoeft, J. T.; Kittel, M.; Woodruff, D. P. *J. Phys. Chem. B* **2004**, *108*, 14316.
(54) Morikawa, Y.; Takahashi, I.; Aizawa, M.; Namai, Y.; Sasaki, T.; Iwasawa, Y. *J. Phys. Chem. B* **2004**, *108*, 14446.
(55) Becke, A. D. *J. Chem. Phys.* **1993**, *98*, 5648.
(56) Lee, C.; Yang, W.; Parr, R. G. *Phys. Rev. B* **1989**, *37*, 785.
(57) Dunning, J.; T. H.; Hay, P. J. In *Modern Theoretical Chemistry*; Plenum: New York, 1977.
(58) Frisch, M. J.; Trucks, G. W.; Schlegel, H. B.; Scuseria, G. E.; Robb, M. A.; Cheeseman, J. R.; Zakrzewski, V. G.; Montgomery, Jr., J. A.; Stratmann, R. E.; Burant, J. C.; Dapprich, S.; Millam, J. M.; Daniels, A. D.; Kudin, K. N.; Strain, M. C.; Farkas, O.; Tomasi, J.; Barone, V.; Cossi, M.; Cammi, R.; Mennucci, B.; Pomelli, C.; Adamo, C.; Clifford, S.; Ochterski, J.; Petersson, G. A.; Ayala, P. Y.; Cui, Q.; Morokuma, K.; Malick, D. K.; Rabuck, A. D.; Raghavachari, K.; Foresman, J. B.; Cioslowski, J.; Ortiz, J. V.; Stefanov, B. B.; Liu, G.; Liashenko, A.; Piskorz, P.; Komaromi, I.; Gomperts, R.; Martin, R. L.; Fox, D. J.; Keith, T.; Al-Laham, M. A.; Peng, C. Y.; Nanayakkara, A.; Gonzalez, C.; Challacombe, M.; Gill, P. M. W.; Johnson, B.; Chen, W.; Wong, M. W.; Andres, J. L.; Gonzalez, C.; Head-Gordon, M.; Replogle, E. S.; Pople, J. A. *Gaussian03*; Gaussian, Inc.: Pittsburgh, 2003.
(59) Scott, A. P.; Radom, L. *J. Phys. Chem.* **1996**, *100*, 16502.